Search for $\eta_c(2S)h_c \to p\bar{p}$ decays and measurements of the $\chi_{cJ} \to p\bar{p}$ branching fractions

M. Ablikim,[1] M. N. Achasov,[8,*] X. C. Ai,[1] O. Albayrak,[4] D. J. Ambrose,[44] F. F. An,[1] Q. An,[45] J. Z. Bai,[1] R. Baldini Ferroli,[19] Y. Ban,[29] J. V. Bennett,[18] M. Bertani,[19] J. M. Bian,[43] E. Boger,[22,†] O. Bondarenko,[23] I. Boyko,[22] S. Braun,[40] R. A. Briere,[4] H. Cai,[52] X. Cai,[1] O. Cakir,[37] A. Calcaterra,[19] G. F. Cao,[1] S. A. Cetin,[38] J. F. Chang,[1] G. Chelkov,[22,†] G. Chen,[1] H. S. Chen,[1] J. C. Chen,[1] M. L. Chen,[1] S. J. Chen,[27] X. Chen,[1] X. R. Chen,[24] Y. B. Chen,[1] H. P. Cheng,[16] X. K. Chu,[29] Y. P. Chu,[1] D. Cronin-Hennessy,[43] H. L. Dai,[1] J. P. Dai,[1] D. Dedovich,[22] Z. Y. Deng,[1] A. Denig,[21] I. Denysenko,[22] M. Destefanis,[48,50] W. M. Ding,[31] Y. Ding,[25] C. Dong,[28] J. Dong,[1] L. Y. Dong,[1] M. Y. Dong,[1] S. X. Du,[54] J. Fang,[1] S. S. Fang,[1] Y. Fang,[1] L. Fava,[49,50] C. Q. Feng,[45] C. D. Fu,[1] J. L. Fu,[27] O. Fuks,[22,†] Q. Gao,[1] Y. Gao,[36] C. Geng,[45] K. Goetzen,[9] W. X. Gong,[1] W. Gradl,[21] M. Greco,[48,50] M. H. Gu,[1] Y. T. Gu,[11] Y. H. Guan,[1] A. Q. Guo,[28] L. B. Guo,[26] T. Guo,[26] Y. P. Guo,[28] Y. P. Guo,[21] Y. L. Han,[1] F. A. Harris,[42] K. L. He,[1] M. He,[1] Z. Y. He,[28] T. Held,[3] Y. K. Heng,[1] Z. L. Hou,[1] C. Hu,[26] H. M. Hu,[1] J. F. Hu,[40] T. Hu,[1] G. M. Huang,[5] G. S. Huang,[45] J. S. Huang,[14] L. Huang,[1] X. T. Huang,[31] Y. Huang,[27] T. Hussain,[47] C. S. Ji,[45] Q. Ji,[1] Q. P. Ji,[28] X. B. Ji,[1] X. L. Ji,[1] L. L. Jiang,[1] X. S. Jiang,[1] J. B. Jiao,[31] Z. Jiao,[16] D. P. Jin,[1] S. Jin,[1] F. F. Jing,[36] T. Johansson,[51] N. Kalantar-Nayestanaki,[23] X. L. Kang,[1] M. Kavatsyuk,[23] B. Kloss,[21] B. Kopf,[3] M. Kornicer,[42] W. Kuehn,[40] A. Kupsc,[51] W. Lai,[1] J. S. Lange,[40] M. Lara,[18] P. Larin,[13] M. Leyhe,[3] C. H. Li,[1] Cheng Li,[45] Cui Li,[45] D. Li,[17] D. M. Li,[54] F. Li,[1] G. Li,[1] H. B. Li,[1] J. C. Li,[1] K. Li,[31] K. Li,[12] Lei Li,[1] P. R. Li,[41] Q. J. Li,[1] T. Li,[31] W. D. Li,[1] W. G. Li,[1] X. L. Li,[31] X. N. Li,[1] X. Q. Li,[28] X. R. Li,[30] Z. B. Li,[35] H. Liang,[45] Y. F. Liang,[33] Y. T. Liang,[40] G. R. Liao,[36] D. X. Lin,[13] B. J. Liu,[1] C. L. Liu,[4] C. X. Liu,[1] F. H. Liu,[32] Fang Liu,[1] Feng Liu,[5] H. B. Liu,[11] H. H. Liu,[15] H. M. Liu,[1] J. Liu,[1] J. P. Liu,[52] K. Liu,[36] K. Y. Liu,[25] P. L. Liu,[31] Q. Liu,[41] S. B. Liu,[45] X. Liu,[24] Y. B. Liu,[28] Z. A. Liu,[1] Zhiqiang Liu,[1] Zhiqing Liu,[21] H. Loehner,[23] X. C. Lou,[1,‡] G. R. Lu,[14] H. J. Lu,[16] H. L. Lu,[1] J. G. Lu,[1] X. R. Lu,[41] Y. Lu,[1] Y. P. Lu,[1] C. L. Luo,[26] M. X. Luo,[53] T. Luo,[42] X. L. Luo,[1] M. Lv,[1] F. C. Ma,[25] H. L. Ma,[1] Q. M. Ma,[1] S. Ma,[1] T. Ma,[1] X. Y. Ma,[1] F. E. Maas,[13] M. Maggiora,[48,50] Q. A. Malik,[47] Y. J. Mao,[29] Z. P. Mao,[1] J. G. Messchendorp,[23] J. Min,[1] T. J. Min,[1] R. E. Mitchell,[18] X. H. Mo,[1] Y. J. Mo,[5] H. Moeini,[23] C. Morales Morales,[13] K. Moriya,[18] N. Yu. Muchnoi,[8,*] Y. Nefedov,[22] I. B. Nikolaev,[8,*] Z. Ning,[1] S. Nisar,[7] X. Y. Niu,[1] S. L. Olsen,[30] Q. Ouyang,[1] S. Pacetti,[20] M. Pelizaeus,[3] H. P. Peng,[45] K. Peters,[9] J. L. Ping,[26] R. G. Ping,[1] R. Poling,[43] E. Prencipe,[21] M. Qi,[27] S. Qian,[1] C. F. Qiao,[41] L. Q. Qin,[31] X. S. Qin,[1] Y. Qin,[29] Z. H. Qin,[1] J. F. Qiu,[1] K. H. Rashid,[47] C. F. Redmer,[21] M. Ripka,[21] G. Rong,[1] X. D. Ruan,[11] A. Sarantsev,[22,§] K. Schönning,[51] S. Schumann,[21] W. Shan,[29] M. Shao,[45] C. P. Shen,[2] X. Y. Shen,[1] H. Y. Sheng,[1] M. R. Shepherd,[18] W. M. Song,[1] X. Y. Song,[1] S. Spataro,[48,50] B. Spruck,[40] G. X. Sun,[1] J. F. Sun,[14] S. S. Sun,[1] Y. J. Sun,[45] Y. Z. Sun,[1] Z. J. Sun,[1] Z. T. Sun,[45] C. J. Tang,[33] X. Tang,[1] I. Tapan,[39] E. H. Thorndike,[44] D. Toth,[43] M. Ullrich,[40] I. Uman,[38] G. S. Varner,[42] B. Wang,[28] D. Wang,[29] D. Y. Wang,[29] K. Wang,[1] L. L. Wang,[1] L. S. Wang,[1] M. Wang,[31] P. Wang,[1] P. L. Wang,[1] Q. J. Wang,[1] S. G. Wang,[29] W. Wang,[1] X. F. Wang,[36] Y. D. Wang,[19] Y. F. Wang,[1] Y. Q. Wang,[21] Z. Wang,[1] Z. G. Wang,[1] Z. H. Wang,[45] Z. Y. Wang,[1] D. H. Wei,[10] J. B. Wei,[29] P. Weidenkaff,[21] S. P. Wen,[1] M. Werner,[40] U. Wiedner,[3] M. Wolke,[51] L. H. Wu,[1] N. Wu,[1] W. Wu,[28] Z. Wu,[1] L. G. Xia,[36] Y. Xia,[17] D. Xiao,[1] Z. J. Xiao,[26] Y. G. Xie,[1] Q. L. Xiu,[1] G. F. Xu,[1] L. Xu,[1] Q. J. Xu,[12] Q. N. Xu,[41] X. P. Xu,[34] Z. Xue,[1] L. Yan,[45] W. B. Yan,[45] W. C. Yan,[45] Y. H. Yan,[17] H. X. Yang,[1] Y. Yang,[5] Y. X. Yang,[10] H. Ye,[1] M. Ye,[1] M. H. Ye,[6] B. X. Yu,[1] C. X. Yu,[28] H. W. Yu,[29] J. S. Yu,[24] S. P. Yu,[31] C. Z. Yuan,[1] W. L. Yuan,[27] Y. Yuan,[1] A. A. Zafar,[47] A. Zallo,[19] S. L. Zang,[27] Y. Zeng,[17] B. X. Zhang,[1] B. Y. Zhang,[1] C. Zhang,[27] C. B. Zhang,[17] C. C. Zhang,[1] D. H. Zhang,[1] H. H. Zhang,[35] H. Y. Zhang,[1] J. J. Zhang,[1] J. L. Zhang,[1] J. Q. Zhang,[1] J. W. Zhang,[1] J. Y. Zhang,[1] J. Z. Zhang,[1] S. H. Zhang,[1] X. J. Zhang,[1] X. Y. Zhang,[31] Y. Zhang,[1] Y. H. Zhang,[1] Z. H. Zhang,[5] Z. P. Zhang,[45] Z. Y. Zhang,[52] G. Zhao,[1] J. W. Zhao,[1] Lei Zhao,[45] Ling Zhao,[1] M. G. Zhao,[28] Q. Zhao,[1] Q. W. Zhao,[1] S. J. Zhao,[54] T. C. Zhao,[1] X. H. Zhao,[27] Y. B. Zhao,[1] Z. G. Zhao,[45] A. Zhemchugov,[22,†] B. Zheng,[46] J. P. Zheng,[1] Y. H. Zheng,[41] B. Zhong,[26] L. Zhou,[1] Li Zhou,[28] X. Zhou,[52] X. K. Zhou,[41] X. R. Zhou,[45] X. Y. Zhou,[1] K. Zhu,[1] K. J. Zhu,[1] X. L. Zhu,[36] Y. C. Zhu,[45] Y. S. Zhu,[1] Z. A. Zhu,[1] J. Zhuang,[1] B. S. Zou,[1] and J. H. Zou[1]

(BESIII Collaboration)

[1]*Institute of High Energy Physics, Beijing 100049, People's Republic of China*
[2]*Beihang University, Beijing 100191, People's Republic of China*
[3]*Bochum Ruhr-University, D-44780 Bochum, Germany*
[4]*Carnegie Mellon University, Pittsburgh, Pennsylvania 15213, USA*

[5]*Central China Normal University, Wuhan 430079, People's Republic of China*
[6]*China Center of Advanced Science and Technology, Beijing 100190, People's Republic of China*
[7]*COMSATS Institute of Information Technology, Lahore, Defence Road, Off Raiwind Road, 54000 Lahore, Pakistan*
[8]*G.I. Budker Institute of Nuclear Physics SB RAS (BINP), Novosibirsk 630090, Russia*
[9]*GSI Helmholtzcentre for Heavy Ion Research GmbH, D-64291 Darmstadt, Germany*
[10]*Guangxi Normal University, Guilin 541004, People's Republic of China*
[11]*GuangXi University, Nanning 530004, People's Republic of China*
[12]*Hangzhou Normal University, Hangzhou 310036, People's Republic of China*
[13]*Helmholtz Institute Mainz, Johann-Joachim-Becher-Weg 45, D-55099 Mainz, Germany*
[14]*Henan Normal University, Xinxiang 453007, People's Republic of China*
[15]*Henan University of Science and Technology, Luoyang 471003, People's Republic of China*
[16]*Huangshan College, Huangshan 245000, People's Republic of China*
[17]*Hunan University, Changsha 410082, People's Republic of China*
[18]*Indiana University, Bloomington, Indiana 47405, USA*
[19]*INFN Laboratori Nazionali di Frascati, I-00044 Frascati, Italy*
[20]*INFN and University of Perugia, I-06100 Perugia, Italy*
[21]*Johannes Gutenberg University of Mainz, Johann-Joachim-Becher-Weg 45, D-55099 Mainz, Germany*
[22]*Joint Institute for Nuclear Research, 141980 Dubna, Moscow region, Russia*
[23]*KVI, University of Groningen, NL-9747 AA Groningen, Netherlands*
[24]*Lanzhou University, Lanzhou 730000, People's Republic of China*
[25]*Liaoning University, Shenyang 110036, People's Republic of China*
[26]*Nanjing Normal University, Nanjing 210023, People's Republic of China*
[27]*Nanjing University, Nanjing 210093, People's Republic of China*
[28]*Nankai university, Tianjin 300071, People's Republic of China*
[29]*Peking University, Beijing 100871, People's Republic of China*
[30]*Seoul National University, Seoul 151-747, Korea*
[31]*Shandong University, Jinan 250100, People's Republic of China*
[32]*Shanxi University, Taiyuan 030006, People's Republic of China*
[33]*Sichuan University, Chengdu 610064, People's Republic of China*
[34]*Soochow University, Suzhou 215006, People's Republic of China*
[35]*Sun Yat-Sen University, Guangzhou 510275, People's Republic of China*
[36]*Tsinghua University, Beijing 100084, People's Republic of China*
[37]*Ankara University, Dogol Caddesi, 06100 Tandogan, Ankara, Turkey*
[38]*Dogus University, 34722 Istanbul, Turkey*
[39]*Uludag University, 16059 Bursa, Turkey*
[40]*Universitaet Giessen, D-35392 Giessen, Germany*
[41]*University of Chinese Academy of Sciences, Beijing 100049, People's Republic of China*
[42]*University of Hawaii, Honolulu, Hawaii 96822, USA*
[43]*University of Minnesota, Minneapolis, Minnesota 55455, USA*
[44]*University of Rochester, Rochester, New York 14627, USA*
[45]*University of Science and Technology of China, Hefei 230026, People's Republic of China*
[46]*University of South China, Hengyang 421001, People's Republic of China*
[47]*University of the Punjab, Lahore-54590, Pakistan*
[48]*University of Turin, I-10125 Turin, Italy*
[49]*University of Eastern Piedmont, I-15121 Alessandria, Italy*
[50]*INFN, I-10125 Turin, Italy*
[51]*Uppsala University, Box 516, SE-75120 Uppsala, Sweden*
[52]*Wuhan University, Wuhan 430072, People's Republic of China*
[53]*Zhejiang University, Hangzhou 310027, People's Republic of China*
[54]*Zhengzhou University, Zhengzhou 450001, People's Republic of China*

(Received 23 October 2013; published 3 December 2013)

Using a sample of $1.06 \times 10^8 \psi(3686)$ events collected with the BESIII detector at BEPCII, the decays $\eta_c(2S) \to p\bar{p}$ and $h_c \to p\bar{p}$ are searched for, where $\eta_c(2S)$ and h_c are reconstructed in the decay chains $\psi(3686) \to \gamma\eta_c(2S)$, $\eta_c(2S) \to p\bar{p}$ and $\psi(3686) \to \pi^0 h_c$, $h_c \to p\bar{p}$, respectively. No significant signals

*Also at the Novosibirsk State University, Novosibirsk, 630090, Russia
†Also at the Moscow Institute of Physics and Technology, Moscow 141700, Russia
‡Also at University of Texas at Dallas, Richardson, Texas 75083, USA
§Also at the PNPI, Gatchina 188300, Russia

are observed. The upper limits of the product branching fractions are determined to be $\mathcal{B}(\psi(3686) \to \gamma\eta_c(2S)) \times \mathcal{B}(\eta_c(2S) \to p\bar{p}) < 1.4 \times 10^{-6}$ and $\mathcal{B}(\psi(3686) \to \pi^0 h_c) \times \mathcal{B}(h_c \to p\bar{p}) < 1.3 \times 10^{-7}$ at the 90% C.L.. The branching fractions for $\chi_{cJ} \to p\bar{p}$ ($J = 0, 1, 2$) are also measured to be $(24.5 \pm 0.8 \pm 1.3, 8.6 \pm 0.5 \pm 0.5, 8.4 \pm 0.5 \pm 0.5) \times 10^{-5}$, which are the world's most precise measurements.

DOI: 10.1103/PhysRevD.88.112001 PACS numbers: 13.25.Gv, 13.40.Hq, 14.40.Pq

I. INTRODUCTION

Charmonium has been playing an important role in understanding the dynamics of QCD. Despite the success of QCD in many aspects of the strong interaction, the charmonium decay mechanism remains challenging and presents disagreement between experimental data and theoretical predictions [1].

In massless QCD models, the processes $\eta_c/\chi_{c0}/h_c/\eta_c(2S) \to p\bar{p}$ are forbidden by the helicity selection rule [2]. However, the experimental observations of the decays $\eta_c/\chi_{c0} \to p\bar{p}$ [3], as well as h_c formed in the $p\bar{p}$ annihilation [4], indicate substantial contributions due to finite masses. These observations have stimulated many theoretical efforts [5–7]. In Ref. [8], it is pointed out that the branching fraction of $\eta_c(2S) \to p\bar{p}$ with respect to that of $\eta_c \to p\bar{p}$ may serve as a criterion to validate the helicity conservation theorem, and an anomalous decay in $\eta_c(2S)$ might imply the existence of a glueball. For the decay $h_c \to p\bar{p}$, possible large branching fractions are suggested. Authors of Ref. [5] investigate the long distance contribution via charmed hadron loops and predict $\mathcal{B}(h_c \to p\bar{p}) = (1.52 - 1.93) \times 10^{-3}$. In Ref. [6], a branching fraction of $\mathcal{B}(h_c \to p\bar{p}) = (3.2 \pm 0.5) \times 10^{-3}$ is predicted by "factorizing" the initial and the final states.

In this paper, we report on a search for $\eta_c(2S)$ and h_c decays into $p\bar{p}$, where $\eta_c(2S)$ is produced from the $\psi(3686)$ radiative transition, while h_c is produced via the isospin-forbidden process $\psi(3686) \to \pi^0 h_c$. In addition, we measure the decays $\chi_{cJ} \to p\bar{p}$ with $J = 0$, 1, and 2. The analysis is based on an e^+e^- annihilation sample of 1.06×10^8 events taken at $\sqrt{s} = 3.686$ GeV [9]. A 44 pb^{-1} sample taken at $\sqrt{s} = 3.65$ GeV is used to estimate the background contribution from the continuum processes.

II. EXPERIMENT AND DATA SETS

The BESIII detector, described in detail in Ref. [10], has an effective geometrical acceptance of 93% of 4π. A helium-based main drift chamber (MDC) determines the momentum of charged particles measured in a 1 T magnetic field with a resolution 0.5% at 1 GeV/c (the resolutions mentioned in the paper are rms resolutions). The energy loss (dE/dx) is also measured with a resolution better than 6%. An electromagnetic calorimeter (EMC) measures energies and positions of electrons and photons. For 1.0 GeV photons and electrons, the energy resolution is 2.5% in the barrel and 5.0% in the end caps, and the position resolution is 6 mm in the barrel and 9 mm in the end caps. A time-of-flight system (TOF) with a time resolution of 80 ps (110 ps) in the barrel (end cap) is used for particle identification. A muon chamber based on resistive plate chambers with 2 cm position resolution provides information for muon identification.

An inclusive Monte Carlo (MC) sample of 1.06×10^8 $\psi(3686)$ events is used for background studies. The $\psi(3686)$ resonance is produced by the event generator KKMC [11], and the decays are generated by EvtGen [12] with known branching fractions [3], while the unmeasured decays are generated according to the Lundcharm model [13]. Exclusive signal MC samples are generated to determine the detection efficiency and to optimize selection criteria. The $h_c \to p\bar{p}$ and $\eta_c(2S) \to p\bar{p}$ decays are generated according to phase space distributions, and $\chi_{cJ} \to p\bar{p}$ decays are generated with an angular distribution of protons following the form $1 + \alpha\cos^2\theta$ in the χ_{cJ} helicity frame, where α is taken from measured data. GEANT4 is used to simulate events where the measured detector resolutions are taken into consideration [14].

III. EVENT SELECTION AND BACKGROUND ANALYSIS

Each charged track is required to have its point of closest approach to the beam line within 1 cm of the beam line in the radial direction and within 10 cm from the interaction point along the beam direction and to lie within the polar angle coverage of the MDC, $|\cos\theta| < 0.93$ in laboratory frame. The information from the TOF is used to form a likelihood $\mathcal{L}_p$ ($\mathcal{L}_K/\mathcal{L}_\pi$) with a proton (kaon/pion) hypothesis. To identify a track as a proton, the likelihood $\mathcal{L}_p$ is required to be greater than $\mathcal{L}_K$ and $\mathcal{L}_\pi$.

Photons are reconstructed from isolated showers in the EMC which are at least 15 (25) degrees away from the proton (antiproton) candidate. Photon candidates in the barrel ($|\cos\theta| < 0.8$) and in the end cap ($0.86 < |\cos\theta| < 0.92$) must have an energy of at least 25 MeV. Electromagnetic showers close to the EMC boundaries are poorly reconstructed and excluded from this analysis. To suppress electronic noise and energy deposits unrelated to the event, the EMC timing of the photon candidate must be in coincidence with collision events $0 \le t \le 14$ (in units of 50 ns).

In the $\psi(3686) \to \gamma\eta_c(2S)/\chi_{cJ} \to \gamma p\bar{p}$ and $\psi(3686) \to \pi^0 h_c \to \pi^0 p\bar{p} \to \gamma\gamma p\bar{p}$ selection, the candidate events must have two oppositely charged tracks and at least one or two good photons, respectively. To suppress the non-proton backgrounds in selecting the $\gamma p\bar{p}$ final states, both

tracks are required to be positively identified as protons, while for the $\gamma\gamma p\bar{p}$ final states, only one track is required to be a proton. A four-constraint (4C) kinematic fit of $\gamma p\bar{p}$ ($\gamma\gamma p\bar{p}$) candidates is performed to the total initial four-momentum of the colliding beams in order to reduce background and to improve the mass resolution. If more photons than required exist in an event, the best one(s) is (are) selected by minimizing the χ^2_{4C} of the 4C kinematic fit. Events with $\chi^2_{4C} < 40$ are accepted as $\gamma p\bar{p}$ ($\gamma\gamma p\bar{p}$) candidates. For $\gamma\gamma p\bar{p}$ candidates, the invariant mass of the two selected photons is further required to be in the range $0.11\ \mathrm{GeV}/c^2 < M(\gamma\gamma) < 0.15\ \mathrm{GeV}/c^2$.

For the $\psi(3686) \to \gamma\eta_c(2S)/\chi_{cJ} \to \gamma p\bar{p}$ channel, the main backgrounds in the $\eta_c(2S)$ signal region ($3.6\ \mathrm{GeV}/c^2 \le M(p\bar{p}) \le 3.66\ \mathrm{GeV}/c^2$) are $\psi(3686) \to p\bar{p}$ decays combined with a fake photon, or with a photon from initial-state radiation or final-state radiation (FSR) and the continuum process. In the χ_{cJ} signal region ($3.3\ \mathrm{GeV}/c^2 \le M(p\bar{p}) \le 3.6\ \mathrm{GeV}/c^2$), the main backgrounds come from the decays $\psi(3686) \to \pi^0 p\bar{p}$ or the nonresonant process $\psi(3686) \to \gamma p\bar{p}$. Since the energy of the transition photon from $\psi(3686) \to \gamma\eta_c(2S)$ is only 50 MeV, $\psi(3686) \to p\bar{p}$ events can easily fake signal events by combining with a fake photon. With a 4C kinematic fit, those events will produce a peak in the $p\bar{p}$ mass spectrum close to the expected $\eta_c(2S)$ mass. Therefore, a three-constraint (3C) kinematic fit, where the magnitude of the photon momentum is allowed to float, is used to determine signal yields. The 3C fit keeps the $\psi(3686) \to p\bar{p}$ peak at the correct position as the photon momentum tends to zero, and it can separate this background from the $\eta_c(2S)$ signal efficiently as shown in Fig. 1 [15]. The background from the continuum process is studied with the data taken at $\sqrt{s} = 3.65$ GeV. The contribution of the background is found to be negligible.

Background from $\psi(3686) \to \pi^0 p\bar{p}$ is measured by selecting $\pi^0 p\bar{p}$ events from data. The $\pi^0 p\bar{p}$ selection is the same as that for $\psi(3686) \to \pi^0 h_c$, $h_c \to p\bar{p}$. A MC sample of $\psi(3686) \to \pi^0 p\bar{p}$ is generated to determine the efficiencies of the $\gamma p\bar{p}$ selection ($\varepsilon_{\gamma p\bar{p}}$) and the $\pi^0 p\bar{p}$ selection ($\varepsilon_{\pi^0 p\bar{p}}$). The selected $\pi^0 p\bar{p}$ events corrected by the efficiencies ($\varepsilon_{\gamma p\bar{p}}/\varepsilon_{\pi^0 p\bar{p}}$) are taken as the $\pi^0 p\bar{p}$ background in $\psi(3686) \to \gamma p\bar{p}$. The shape of this background can be described with a Novosibirsk function [16] as shown in Fig. 2.

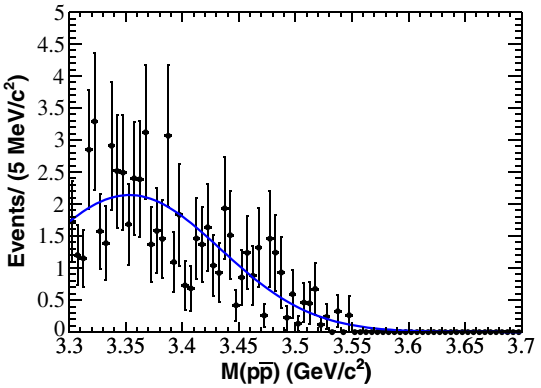

FIG. 2 (color online). The measured background from $\psi(3686) \to \pi^0 p\bar{p}$ for the $\psi(3686) \to \gamma p\bar{p}$ mode. The curve shows the fit with a Novosibirsk function.

For $\psi(3686) \to \pi^0 h_c \to \pi^0 p\bar{p}$, the main background sources are the decays $\psi(3686) \to \gamma\chi_{cJ}$, $\chi_{cJ} \to p\bar{p}$ (where $J = 1, 2$) combined with a fake photon and the $\pi^0 p\bar{p}$ decay from $\psi(3686)$ or continuum process. The χ_{cJ} backgrounds are strongly suppressed by using the 3C kinematic fit, where the momentum of the photon with lower energy is allowed to float. For the χ_{cJ} backgrounds, the $M(p\bar{p}\gamma_{\mathrm{high}})$ (where γ_{high} is the photon with higher energy) with 3C peaks at $3.686\ \mathrm{GeV}/c^2$, while for the h_c signal, it is below $3.66\ \mathrm{GeV}/c^2$ as shown in Fig. 3 [15]. A requirement $M(p\bar{p}\gamma_{\mathrm{high}}) < 3.66\ \mathrm{GeV/c^2}$ is used to remove this background effectively. The $\pi^0 p\bar{p}$ background from the

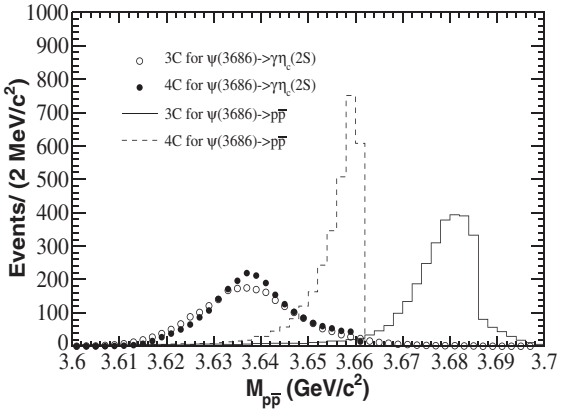

FIG. 1. Comparison of the invariant mass $M(p\bar{p})$ between 3C and 4C kinematic fits. For $\psi(3686) \to \gamma\eta_c(2S)$, the open and filled circles are corresponding to 3C and 4C, and for $\psi(3686) \to p\bar{p}$, the solid and dashed lines are for 3C and 4C, respectively.

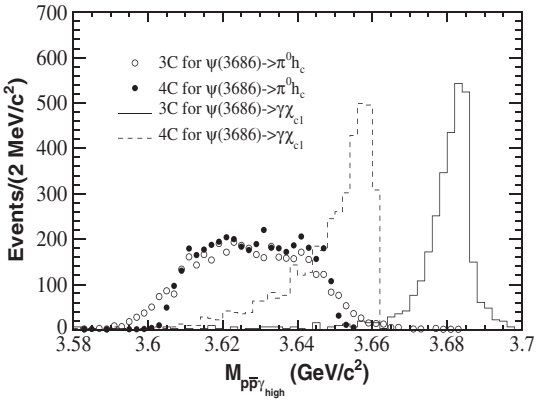

FIG. 3. Comparison of the invariant mass $M(p\bar{p}\gamma_{\mathrm{high}})$ between 3C and 4C kinematic fits. For $\psi(3686) \to \pi^0 h_c$, the open and filled circles are corresponding to 3C and 4C, and for $\psi(3686) \to \gamma\chi_{c1}$, the solid and dashed lines are for 3C and 4C, respectively.

continuum process is studied with the data sample taken at $\sqrt{s} = 3.65$ GeV and is found not peaking in the signal region. The $\pi^0 p\bar{p}$ background having the same final state as signal events is irreducible. It is included in the fit to the $M(p\bar{p})$ spectrum.

IV. DETERMINATION OF YIELDS

Figure 4 shows the $p\bar{p}$ invariant-mass distribution for the selected $\gamma p\bar{p}$ candidates. There are clear χ_{c0}, χ_{c1}, χ_{c2}, and $\psi(3686) \to p\bar{p}$ peaks. The signal for $\eta_c(2S) \to p\bar{p}$ is not significant. An unbinned maximum likelihood fit to the $M(p\bar{p})$ distribution is used to determine the signal yields of $\eta_c(2S)$ and χ_{cJ}. The fitting function is composed of signal and background components, where the signal components include $\eta_c(2S)$ and χ_{cJ}, and the background components include $\pi^0 p\bar{p}$, $\psi(3686) \to p\bar{p}$, $\psi(3686) \to \gamma_{\rm FSR} p\bar{p}$ and nonresonant background. The line shapes for $\eta_c(2S)$ and χ_{cJ} are obtained from MC simulation following $E_\gamma^3 \times BW(m; m_0, \Gamma) \times f_{\rm damp}(E_\gamma)$, where m is the invariant mass of $p\bar{p}$, m_0 and Γ are the mass and width of the Breit–Wigner line shape for $\eta_c(2S)$ and χ_{cJ}, and the values are fixed at the nominal values [3]. E_γ [which equals $(m^2_{\psi(3686)} - m^2)/2m_{\psi(3686)}$] is the energy of the transition photon in the rest frame of $\psi(3686)$, and $f_{\rm damp}(E_\gamma)$ is a function that damps the diverging tail originating from the E_γ^3 dependence at the low mass side (corresponding to high energy of the radiative photon). The form of the damping factor was introduced by the KEDR collaboration and is $f_{\rm damp}(E_\gamma) = \frac{E_0^2}{E_\gamma E_0 + (E_\gamma - E_0)^2}$ [17], where E_0 is the peak energy of the transition photon. The $\pi^0 p\bar{p}$ background is described with a Novosibirsk function with the fixed shape and amplitude as described earlier. The backgrounds from

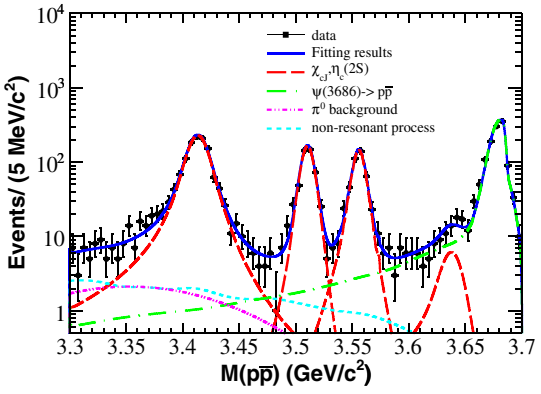

FIG. 4 (color online). The $p\bar{p}$ invariant-mass spectrum after a 3C kinematic fit for selected $\psi(3686) \to \gamma p\bar{p}$ candidates from data. Dots with error bars are data, the blue solid curve is the fitting result, the red long-dashed line is for the χ_{cJ} and $\eta_c(2S)$ signals, the green long-dash-dotted line is for $\psi(3686) \to p\bar{p}$, the pink dash-double-dotted line is the contribution of $\psi(3686) \to \pi^0 p\bar{p}$ and the cyan dashed line is for the nonresonant process.

$\psi(3686) \to p\bar{p}$ and $\psi(3686) \to p\bar{p}\gamma_{\rm FSR}$ are described with a shape based on a MC simulation, where the FSR photon is simulated with PHOTOS [18], and their magnitudes are allowed to float. The shape of the nonresonant background is determined from a MC simulation, while its magnitude is allowed to float. To account for a possible difference in the mass resolution between data and MC simulation, a smearing Gaussian function $G(\mu, \sigma)$ is convolved with the line shape of χ_{cJ}, and the parameters of this function are free in the fit. Since we find that the discrepancy in the mass resolution decreases with increasing $M(p\bar{p})$ and is close to zero in the $\eta_c(2S)$ region, a MC-determined line shape is directly used for the $\eta_c(2S)$ in the fit to data. The fitting results are shown in Fig. 4. The signal yields of χ_{c0}, χ_{c1}, χ_{c2}, and $\eta_c(2S)$ are 1222 ± 39, 453 ± 23, 405 ± 21, and 34 ± 17, respectively. The statistical significance of the $\eta_c(2S)$ signal is 1.7σ. The goodness of fit is $\chi^2/ndf = 50.8/65$, which indicates a reasonable fit.

Since $\eta_c(2S)$ signal is not significant, we determine the upper limit on the number of signal events. The probability density function (PDF) for the expected number of signal events is taken to be the likelihood in fitting the $M(p\bar{p})$ distribution while scanning the number of $\eta_c(2S)$ signal events from zero to a large number, where the signal yields of the χ_{cJ} are free. The 90% C.L. upper limit on the number of signal events $N^{\rm up}$, which corresponds to $\int_0^{N^{\rm up}} {\rm PDF}(x)dx / \int_0^{\infty} {\rm PDF}(x)dx = 0.9$, is 54.

Figure 5 shows the $p\bar{p}$ invariant-mass distribution for the selected $\psi(3686) \to \pi^0 p\bar{p}$ candidates. There is no obvious $h_c \to p\bar{p}$ signal. The signal yield of h_c is determined from an unbinned maximum-likelihood fit to the $M(p\bar{p})$ distribution in $\psi(3686) \to \pi^0 p\bar{p}$ with the signal and the $\pi^0 p\bar{p}$ background components. The h_c signal is described by the MC determined shape convolved with a smearing Gaussian. In the MC simulation, the mass and width of h_c are set to the measured values [3]. The smearing Gaussian is used to account for the difference in the

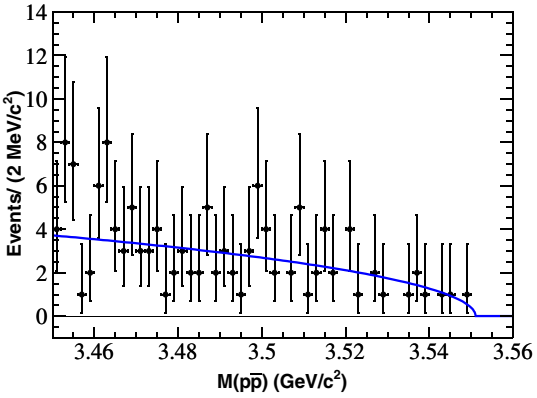

FIG. 5 (color online). The $p\bar{p}$ invariant-mass spectrum for $\psi(3686) \to \pi^0 p\bar{p}$. Dots with error bars are data, and the blue solid curve is the fitting result with the background shape.

mass resolution between data and MC simulation. The parameters of the Gaussian function are determined from $\psi(3686) \to \pi^0 J/\psi \to \pi^0 p\bar{p}$. The $\pi^0 p\bar{p}$ background is described by an ARGUS function [19] with the magnitude and shape parameters floated. No obvious h_c signal event is observed. The upper limit at the 90% C.L. on the $h_c \to p\bar{p}$ signal events, calculated with the same method as was applied for the $\eta_c(2S)$, is 4.4. Figure 5 shows the fitting result with the background shape, and the goodness of fit is $\chi^2/ndf = 18.4/14$.

V. SYSTEMATIC UNCERTAINTIES

In the branching-fraction measurements, there are systematic uncertainties from MDC tracking (1% per track) [20], particle identification (1% per track) [20], photon reconstruction (1% per photon) [21], the total number of $\psi(3686)$ events (0.8%) [9], the kinematic fit, and the simulation of helicity angular distribution of the proton and antiproton. The uncertainty in the kinematic fit comes from the inconsistency between the data and MC simulation of the track-helix parameters. We make corrections to the helix parameters according to the procedure described in Ref. [22] and take the difference between the efficiencies with and without the correction as the systematic error. The helicity angular distribution of protons from χ_{cJ} is taken from measured data and fitted by the formula $1 + \alpha\cos^2\theta$. The α values for χ_{c0}, χ_{c1}, and χ_{c2} are 0.09 ± 0.11, 0.12 ± 0.20, and -0.26 ± 0.17, respectively. The selection efficiencies are determined from MC where the α values are set to the mean values. The change in efficiency by varying the α value by $\pm 1\sigma$ is taken as the uncertainty in the proton angular distribution. For $\eta_c(2S)/h_c \to p\bar{p}$, the differences in efficiencies for MC samples simulated with phase space and $1 + \cos^2\theta$, 0.8% and 0.5% for $\eta_c(2S)$ and h_c, respectively, are taken as the systematic errors.

For the $\mathcal{B}(\eta_c(2S)/\chi_{cJ} \to p\bar{p})$ measurement, the uncertainties in the fitting procedure include the damping factor, fitting range, the description of the π^0 background, and the mass resolution of $M(p\bar{p})$. An alternative damping function $\exp(-E_\gamma^2/8\beta^2)$ was used by CLEO [23], where $\beta = 65.0 \pm 2.5$ and 97 ± 24 MeV for $\eta_c(2S)$ and χ_{cJ}, respectively [22]. The difference in the final results caused by the two damping factors is taken as the systematic uncertainty. The uncertainty caused by the fitting range is obtained by varying the limits of the fitting range by ± 0.05 GeV/c^2. The uncertainty of the π^0 background is estimated by varying the parameters of the shape and magnitude by $\pm 1\sigma$. The uncertainty from the resolution of $M(p\bar{p})$ is found to be negligible.

For $\mathcal{B}(h_c \to p\bar{p})$, additional uncertainties are caused by the mass resolution of $M(p\bar{p})$, the fitting range, the π^0 mass requirement, and the background shape. The uncertainty from the mass resolution of $M(p\bar{p})$ is estimated by varying the resolution by $\pm 1\sigma$. The uncertainty due to the fitting range is estimated by allowing the fitting range to vary within 0.05 GeV/c^2. The difference in the number of h_c signal events is taken as the systematic error. The uncertainty due to the π^0 mass requirement is studied using the decay $\psi(3686) \to \pi^0\pi^0 J/\psi$, $J/\psi \to l^+l^-$ [24], and 3% is quoted as the systematic uncertainty. The uncertainty from the background shape (12.5%) is estimated by changing the background shape from an ARGUS function to a second-order polynomial. Table I summarizes all the systematic uncertainties. The overall systematic uncertainties are obtained by summing all the sources of systematic uncertainties in quadrature, assuming they are independent.

TABLE I. Summary of the relative systematic uncertainties in $\mathcal{B}(\chi_{cJ} \to p\bar{p})$, $\mathcal{B}(\eta_c(2S) \to p\bar{p})$ and $\mathcal{B}(h_c \to p\bar{p})$ (in %).

Source	χ_{c0}	χ_{c1}	χ_{c2}	$\eta_c(2S)$	h_c
Tracking efficiency	2.0	2.0	2.0	2.0	2.0
Photon detection	1.0	1.0	1.0	1.0	2.0
Particle identification	2.0	2.0	2.0	2.0	1.0
Kinematic fit	0.4	0.2	0.6	1.1	1.4
Total number of $\psi(3686)$	0.8	0.8	0.8	0.8	0.8
Damping factor	1.1	0.1	0.2	11.8	···
Fitting range	1.4	0.4	0.2	5.9	3.4
Background shape	0.8	0.9	0.6	8.9	12.5
Proton angle distribution	0.8	0.6	0.3	0.8	0.5
Resolution of $M(p\bar{p})$	···	···	···	···	5.7
π^0 mass region cut	···	···	···	···	3.0
Sum	3.8	3.3	3.2	16.3	14.9

VI. RESULTS AND DISCUSSION

We use MC-determined efficiencies to calculate the product branching fractions $\mathcal{B}(\psi(3686) \to \gamma\chi_{cJ}) \times \mathcal{B}(\chi_{cJ} \to p\bar{p})$. By combining the measurements of $\mathcal{B}(\psi(3686) \to \gamma\chi_{cJ})$ [3], the branching fractions for $\chi_{cJ} \to p\bar{p}$ are obtained. The results are summarized in Table II. The upper limits on the product branching fractions of the $\eta_c(2S)$ and h_c are calculated with the formula $\frac{N^{\rm up}}{N^{\rm tot}\times\varepsilon\times(1-\sigma)}$. Here $N^{\rm up}$ is the upper limit of signal events, $N^{\rm tot}$ is the number of $\psi(3686)$ events, ε is the MC-determined efficiency (45.6% for $\psi(3686) \to \gamma\eta_c(2S) \to \gamma p\bar{p}$, and 37.7% for $\psi(3686) \to \pi^0 h_c \to \pi^0 p\bar{p}$, and σ is the overall systematic error. We obtain $\mathcal{B}(\psi(3686) \to \gamma\eta_c(2S)) \times \mathcal{B}(\eta_c(2S) \to p\bar{p}) < 1.4 \times 10^{-6}$ and $\mathcal{B}(\psi(3686) \to \pi^0 h_c) \times \mathcal{B}(h_c \to p\bar{p}) < 1.3 \times 10^{-7}$ at the 90% C.L.

The branching fraction for $\eta_c(2S) \to p\bar{p}$ is determined by multiplying the ratio of the product branching fractions $\frac{\mathcal{B}(\psi(3686)\to\gamma\eta_c(2S))\times\mathcal{B}(\eta_c(2S)\to p\bar{p})}{\mathcal{B}(\psi(3686)\to\gamma\eta_c(2S))\times\mathcal{B}(\eta_c(2S)\to K\bar{K}\pi)}$ and $\mathcal{B}(\eta_c(2S) \to K\bar{K}\pi)$. Here the product branching fraction $\mathcal{B}(\psi(3686) \to \gamma\eta_c(2S)) \times \mathcal{B}(\eta_c(2S) \to K\bar{K}\pi)$ is taken from the recent BESIII measurement [25], and $\mathcal{B}(\eta_c(2S) \to K\bar{K}\pi)$ was measured by BABAR [26]. This allows some systematic errors, such as errors in the tracking efficiency and the damping factor, to cancel out. The result is inflated by a

TABLE II. The selection efficiencies, signal yields extracted from the fit, the product branching fractions $\mathcal{B}(\psi(3686) \to \gamma\chi_{cJ}) \times \mathcal{B}(\chi_{cJ} \to p\bar{p})$, and the branching fractions $\mathcal{B}(\chi_{cJ} \to p\bar{p})$. Here the first errors are statistical and the second systematic.

Channels	$\varepsilon(\%)$	N_{signal}	$\mathcal{B}(\psi(3686) \to \gamma\chi_{cJ}) \times \mathcal{B}(\chi_{cJ} \to p\bar{p})(\times 10^{-5})$	$\mathcal{B}(\chi_{cJ} \to p\bar{p})(\times 10^{-5})$
χ_{c0}	48.5	1222 ± 39	$2.37 \pm 0.08 \pm 0.09$	$24.5 \pm 0.8 \pm 1.3$
χ_{c1}	53.8	453 ± 23	$0.79 \pm 0.04 \pm 0.03$	$8.6 \pm 0.5 \pm 0.5$
χ_{c2}	52.0	405 ± 21	$0.73 \pm 0.04 \pm 0.03$	$8.4 \pm 0.5 \pm 0.5$

factor $1/(1-\sigma)$, where the fractional systematic error σ is dominated by the $\mathcal{B}(\eta_c(2S) \to K\bar{K}\pi)$ measurement. The 90% C.L. upper limit is determined to be $\mathcal{B}(\eta_c(2S) \to p\bar{p}) < 4.8 \times 10^{-3}$. By combining the BESIII measurement of $\mathcal{B}(\psi(3686) \to \pi^0 h_c)$ [24], the upper limit of the branching fraction is obtained to be $\mathcal{B}(h_c \to p\bar{p}) < 1.7 \times 10^{-4}$ at the 90% C.L., where the errors are treated with the same method as in $\mathcal{B}(\eta_c(2S) \to p\bar{p})$.

In summary, with a sample of $1.06 \times 10^8\, \psi(3686)$ events, we search for the decays $\eta_c(2S) \to p\bar{p}$ and $h_c \to p\bar{p}$, but no significant signals are observed. The 90% C.L. upper limits of the branching fractions for $\eta_c(2S) \to p\bar{p}$ and $h_c \to p\bar{p}$ are determined. The current upper limit of $\mathcal{B}(\eta_c(2S) \to p\bar{p})$, which is larger than the measurement of $\mathcal{B}(\eta_c \to p\bar{p})$ [27], cannot directly test the conjecture of Ref. [8] to validate the helicity theorem. The upper limit on $\mathcal{B}(h_c \to p\bar{p})$ obtained from this work is consistent with the earlier experimental results [4] and is lower than the predictions [5,6], where model parameters may need to be tuned. The branching fractions of $\chi_{cJ} \to p\bar{p}$ are measured with improved precision, consistent with the most recent measurement by CLEO-c [28], and the results are also compatible with theoretical calculation of $\mathcal{B}(\chi_{cJ} \to p\bar{p})$ $(J = 0, 1, 2)$ by including the color octet contribution [29]. The results presented in this paper will be of interest for future experiments like PANDA in their search for hadronic resonances [30].

ACKNOWLEDGMENTS

The BESIII collaboration thanks the staff of BEPCII and the computing center for their strong support. This work is supported in part by the Ministry of Science and Technology of China under Contract No. 2009CB825200; National Natural Science Foundation of China (NSFC) under Contracts No. 10625524, No. 10821063, No. 10825524, No. 10835001, No. 10935007, No. 11125525, and No. 11235011; Joint Funds of the National Natural Science Foundation of China under Contracts No. 11079008 and No. 11179007; the Chinese Academy of Sciences (CAS) Large-Scale Scientific Facility Program; CAS under Contracts No. KJCX2-YW-N29 and No. KJCX2-YW-N45; 100 Talents Program of CAS; German Research Foundation DFG under Collaborative Research Center Contract No. CRC-1044; Istituto Nazionale di Fisica Nucleare, Italy; Ministry of Development of Turkey under Contract No. DPT2006K-120470; U. S. Department of Energy under Contracts No. DE-FG02-04ER41291, No. DE-FG02-05ER41374, No. DE-FG02-94ER40823, and No. DESC0010118; U.S. National Science Foundation; University of Groningen (RuG) and the Helmholtzzentrum fuer Schwerionenforschung GmbH (GSI), Darmstadt; and WCU Program of National Research Foundation of Korea under Contract No. R32-2008-000-10155-0.

[1] E. Eichten, S. Godfrey, H. Mahlke, and J. L. Rosner, Rev. Mod. Phys. **80**, 1161 (2008).
[2] S. J. Brodsky and G. P. Lepage, Phys. Rev. D **24**, 2848 (1981).
[3] J. Beringer *et al.* (Particle Data Group), Phys. Rev. D **86**, 010001 (2012).
[4] M. Andreotti *et al.*, Phys. Rev. D **72**, 032001 (2005).
[5] X. H. Liu and Q. Zhao, J. Phys. G **38**, 035007 (2011).
[6] S. Barsuk, J. He, E. Kou, and B. Viaud, Phys. Rev. D **86**, 034011 (2012).
[7] F. Murgia, Phys. Rev. D **54**, 3365 (1996).
[8] K.-T. Chao, Y.-F. Gu, and S. F. Tuan, Commun. Theor. Phys. **25**, 471 (1996).
[9] M. Ablikim *et al.* (BESIII Collaboration), Chin. Phys. C **37**, 063001 (2013).
[10] M. Ablikim *et al.* (BESIII Collaboration), Nucl. Instrum. Methods Phys. Res., Sect. A **614**, 345 (2010).
[11] S. Jadach, B. F. L. Ward, and Z. Was, Comput. Phys. Commun. **130**, 260 (2000); Phys. Rev. D **63**, 113009 (2001).
[12] http://www.slac.stanford.edu/lange/EvtGen; P. Rong-Gang, Chin. Phys. C **32**, 599 (2008).
[13] J. C. Chen, G. S. Huang, X. R. Qi, D. H. Zhang, and Y. S. Zhu, Phys. Rev. D **62**, 243 (2000).
[14] S. Agostinelli *et al.* (geant4 Collaboration), Nucl. Instrum. Methods Phys. Res., Sect. A **506**, 250 (2003).
[15] M. Ablikim *et al.* (BESIII Collaboration), Phys. Rev. D **84**, 091102 (2011).
[16] The Novosibirsk function is defined as $f(m_{ES}) = A_S \exp(-0.5\ln^2[1 + \Lambda\tau \cdot (m_{ES} - m_0)]/\tau^2 + \tau^2)$, where $\Lambda = \sinh(\tau\sqrt{\ln 4})/(\sigma\tau\sqrt{\ln 4})$, the peak position is m_0, the width is σ, and τ is the tail parameter.

[17] V. V. Anashin, Int. J. Mod. Phys. Conf. Ser. **02**, 188 (2011).
[18] E. Barberio and Z. Was, Comput. Phys. Commun. **79**, 291 (1994).
[19] H. Albrecht *et al.* (ARGUS Collaboration), Phys. Lett. B **241**, 278 (1990).
[20] M. Ablikim *et al.* (BESIII Collaboration), Phys. Rev. D **86**, 032014 (2012).
[21] M. Ablikim *et al.* (BESIII Collaboration), Phys. Rev. D **83**, 112005 (2011).
[22] M. Ablikim *et al.* (BESIII Collaboration), Phys. Rev. D **87**, 012002 (2013).
[23] R. E. Mitchell *et al.* (CLEO Collaboration), Phys. Rev. Lett. **102**, 011801 (2009).
[24] M. Ablikim *et al.* (BESIII Collaboration), Phys. Rev. Lett. **104**, 132002 (2010).
[25] M. Ablikim *et al.* (BESIII Collobration), Phys. Rev. Lett. **109**, 042003 (2012).
[26] B. Aubert *et al.* (*BABAR* Collaboration), Phys. Rev. D **78**, 012006 (2008).
[27] M. Ablikim *et al.* (BESIII Collaboration), Phys. Rev. D **86**, 092009 (2012).
[28] P. Naik *et al.* (CLEO Collaboration), Phys. Rev. D **78**, 031101(R) (2008).
[29] S. M. H. Wong, Eur. Phys. J. C **14**, 643 (2000).
[30] A. Lundborg, T. Barnes, and U. Wiedner, Phys. Rev. D **73**, 096003 (2006).